Day-night Contrast in the Cloud Water Responses to Aerosols

J. Rahu[1], H. Trofimov[1], P. Post[1], and V. Toll[1]

[1] Laboratory of Atmospheric Physics, University of Tartu, Tartu, Estonia.

Corresponding authors: Jorma Rahu (jorma.rahu@ut.ee), Velle Toll (velle.toll@ut.ee)

Key Points:

- We demonstrated that geostationary satellite data could be used to study the temporal evolution of pollution tracks
- Geostationary satellite data indicated that in continental pollution tracks cloud water decreases during night time
- Cloud water increases in the afternoon, most likely due to suppression of precipitation
-

Abstract

Clouds play an essential role in the global energy budget but the impact of anthropogenic aerosols on clouds is still poorly understood. We use fifteen-minute temporal resolution geostationary satellite data to study the temporal evolution of polluted cloud tracks detected in the European part of Russia. Previous analysis of polluted cloud tracks shows that cloud water response to aerosols is bidirectional. Here, we show that the day-night contrast in cloud responses partly explains the bidirectional cloud water responses. We have data only for sunlight hours, but we can interpret the cloud responses detected already since the early morning as night-time responses. On average, the decrease in cloud water offsets 46% of the Twomey effect in the study area while the decrease happens during night-time, probably due to aerosol-enhanced entrainment. In the afternoon, cloud water is more likely to increase in the polluted clouds, most probably due to suppressed precipitation. Our findings highlight the need to better account for the temporal evolution of cloud responses to estimate the aerosol radiative forcing more accurately.

Plain Language Summary

The global warming induced by anthropogenic greenhouse gases is partly compensated by the aerosol cooling effect while the extent of aerosol cooling is still relatively uncertain. Lately, the analysis of clouds polluted by isolated aerosol sources like isolated factories has provided new insights into aerosol influence on clouds and the resulting cooling effect. Here, we use geostationary satellite data to study the temporal evolution of continental clouds polluted by localized heavy industrial emissions. Polluted clouds become thinner compared to nearby unpolluted clouds during the night. Some of the polluted clouds become thicker compared to the nearby unpolluted clouds in the afternoon. These results improve the process-level understanding of anthropogenic aerosol impacts on clouds.

1 Introduction

Not only anthropogenic greenhouse gases but also microscopic anthropogenic air pollution particles called aerosols influence Earth's climate. Despite strong research efforts, the aerosol forcing of Earth's climate is still poorly quantified compared to the greenhouse gas (GHG) induced forcing (Bellouin et al., 2020). Considering multiple lines of evidence, total aerosol effective radiative forcing is estimated to be from -2.0 to -0.4 $\frac{W}{m^2}$ with a 90% likelihood (Bellouin et al., 2020). The fact that aerosols offset a poorly quantified fraction of GHG-induced global warming, makes it challenging to estimate the sensitivity of the Earth's climate to anthropogenic radiative forcing (Stevens et al., 2016) and to improve the reliability of climate projections.

Besides the direct radiative interactions, aerosols act as cloud condensation nuclei (CCN) and therefore modulate cloud properties. The climate forcing caused by aerosol impacts on clouds is especially poorly quantified (Bellouin et al., 2020). The first indirect effect of aerosols, also called the Twomey effect (Twomey, 1974), refers to increased cloud droplet number concentration (CDNC) in clouds. Twomey effect raises the cloud albedo and therefore induces a cooling effect on the Earth's climate. The Twomey effect is well understood and the cooling effect is confirmed by multiple lines of evidence (Bellouin et al., 2020).

The second aerosol indirect effect concerns the liquid water path (LWP) and cloud fraction response to increased CDNC (Albrecht, 1989; IPCC, 2013). LWP can increase due to suppressed collision-coalescence efficiency leading to suppressed precipitation (Albrecht, 1989) and decrease due to aerosol-enhanced entrainment (Ackerman et al., 2004; Bretherton et al., 2007; Wood, 2007). But the net cloud water response to aerosols remains relatively poorly constrained (Bellouin et al., 2020).

Polluted cloud tracks – quasi-linear polluted cloud lines induced by localized pollution sources – have recently provided more stringent constraint on LWP response to aerosols (Toll et al., 2019). Polluted cloud tracks allow us to directly compare the polluted cloud properties with the properties of the unpolluted clouds as the pollution tracks stand out from the less polluted background. While global climate models assume unidirectional LWP increases (Ghan et al., 2016), polluted cloud tracks show bidirectional responses (Toll et al., 2017). Using ship, volcano, industry and fire tracks, Toll et al. (2019) found that on average there is a weak decrease in LWP, partially cancelling out the Twomey effect. Trofimov et al. (2020) found bidirectional LWP responses with weak average LWP response also in the case of larger-scale cloud perturbations. Previous studies on polluted cloud tracks use data from polar-orbiting satellites (Toll et al., 2019, 2017; Trofimov et al., 2020), enabling to analyse only snapshots of cloud responses.

In this paper, we analyse the temporal evolution of LWP responses using polluted cloud tracks detected from the geostationary Spinning Enhanced Visible and Infrared Imager (SEVIRI) satellite data in the European part of Russia. Gryspeerdt et al. (2020) found a clear temporal evolution of LWP response in ship tracks with a more likely increase in LWP after 10 hours since the initial cloud droplet number perturbation. Diamond et al. (2020) found a clear decrease in LWP in the South-East Atlantic shipping corridor in the afternoon, but a weak LWP response in the morning. Diurnal evolution observed over ocean motivates to analyse the diurnal evolution of LWP response also over land. Glassmeier et al. (2021) suggested that the characteristic cloud water adjustment equilibration time scale in non-precipitating clouds is 20 hours, which should allow us to observe the evolution towards equilibrium state using SEVIRI data. We study if we can capture the temporal evolution of bidirectional cloud water responses and check the existence of the day-night contrast in the cloud water response.

96 ## 2 Data and Methods

97

98 ### 2.1 General study design

99

100 We use SEVIRI and Moderate Resolution Imaging Spectroradiometer (MODIS) data to compare
101 the properties of the polluted clouds to the properties of the nearby unpolluted clouds. Using
102 SEVIRI data, we study polluted cloud tracks affected by anthropogenic aerosols originating from
103 various industrial sources in the European part of Russia (Fig 1 and Table 1). The studied aerosol
104 sources include various chemical and heavy production industries as well as mines (Table 1).
105 These strong and localised pollution sources in relatively clean background conditions often
106 provide a clear contrast between polluted and unpolluted clouds (example in Fig 2). In total, we
107 study 23 days with distinct visible pollution tracks in the years 2006 to 2017 (Table 2) using
108 SEVIRI data. From these 23 cases, we extracted the time-series of 74 individual pollution tracks
109 with different temporal and geographical extents. We focus especially on the temporal evolution
110 of cloud water response to aerosols.

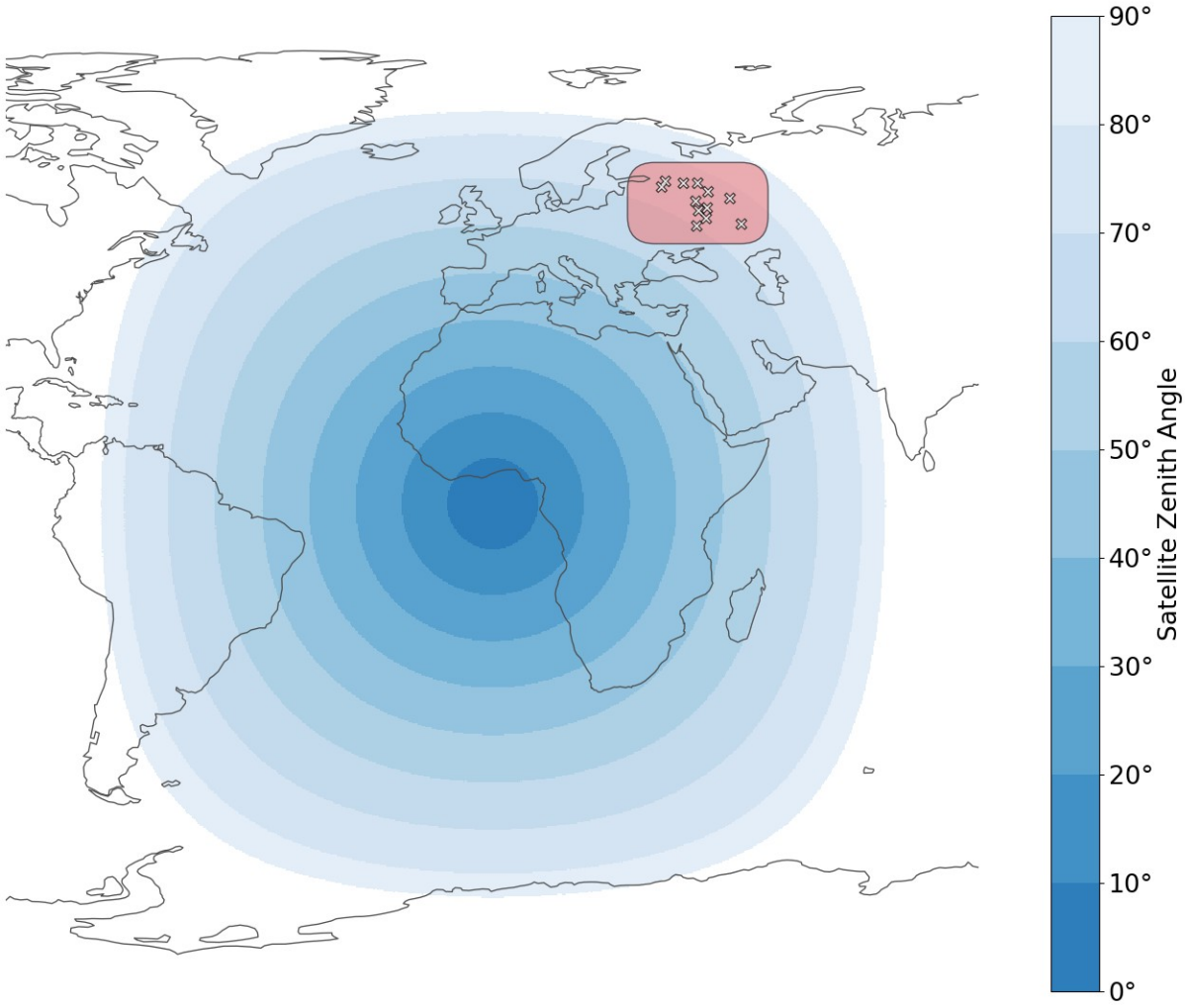

Figure 1. The dependence of spatial resolution of SEVIRI data on geographical location. The spatial resolution of the SEVIRI data decreases further away from the 0º longitude and 0º latitude. The red box marks the approximate area where pollution tracks were observed. Crosses mark the largest industrial sites in the area from where pollution tracks were often originating.

Table 1. List of cities with heavy industry, from where sampled pollution tracks originated.

City	(latitude, longitude)	Type of industry
Cherepovets	(59.13, 37.92)	metallurgy and chemical industry
Yaroslavl	(57.62, 39.85)	machine factory
Chagoda	(59.17, 35.33)	glass factory
Ryazan	(54.60, 39.70)	electronics factory and oil refinery
Kirishi	(59.45, 32.02)	oil refinery and chemical industry
Novomoskovsk	(54.08, 38.22)	chemical industry

Moscow	(55.75, 37.62)	chemical, textile and car-building industry
Veliky Novgorod	(58.52, 31.28)	chemical and radio-electronic industry
Lipetsk	(52.62, 39.60)	metallurgy, machinery, chemical industry
Stary Oskol	(51.30, 37.83)	iron ore mine
Nizhny Novgorod	(56.33, 44.01)	auto industry, ship, and aircraft factories
Saratov	(51.53, 46.02)	oil refinery, aerospace manufacturing industry

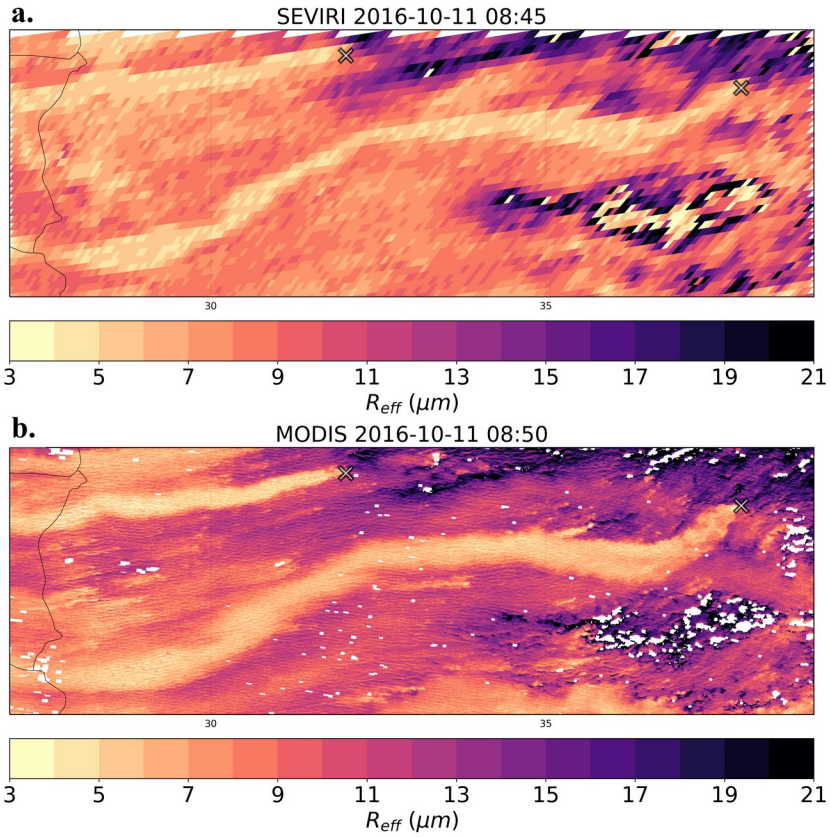

Figure 2. An example of cloud droplet effective radius (R_{eff} ¿ data from two different satellite instruments: **a.** SEVIRI, **b.** MODIS. Yellowish wavy areas with reduced droplet sizes represent pollution tracks originating from cities with heavy industry. The pollution tracks can span over several hundred kilometres downwind of emission sources. Although the spatial resolution is lower for SEVIRI data and the contrast between polluted and unpolluted areas is lower, the tracks are still clearly visible.

Table 2. List of dates for which tracks were sampled. The number of tracks sampled for each date is given in the parentheses.

2006 (5)	2007 (4)	2008 (12)	2009 (3)	2011 (10)	2015 (8)	2016 (26)	2017 (6)

10-16 (3)	04-29 (2)	09-16 (7)	10-25 (3)	10-24 (4)	02-13 (3)	10-10 (6)	10-01 (6)
10-26 (2)	10-16 (2)	09-17 (2)		10-27 (1)	02-14 (3)	10-11 (6)	
		09-18 (2)		11-02 (2)	10-20 (2)	10-12 (3)	
		11-06 (1)		11-13 (3)		10-13 (4)	
						10-16 (4)	
						10-19 (3)	

As SEVIRI is onboard geostationary satellite, continuous temporal coverage of cloud properties during each day is available. As the MODIS instrument is onboard polar-orbiting Terra and Aqua satellites, we get snapshots of clouds during various times of the day depending on the location. We use MODIS data from Toll et al. (2019) from various continental sites in Russia, Canada, and Australia. As both SEVIRI and MODIS are passive instruments, we can study cloud responses during sunlight hours only. To compare the diurnal evolution in cloud responses between MODIS and SEVIRI data, we used normalized time-coordinate, where 0 is the local sunrise, 0.5 is the local noon, and 1 represents the local sunset.

We compare the changes in cloud optical depth (COD) to the changes in cloud droplet effective radius (R_{eff}) to study the changes in LWP. We assume the following relationship between COD, LWP and R_{eff}

$$COD \quad \frac{LWP}{R_{eff}}. \tag{1}$$

From this, we derive a relation between logarithmic changes of LWP and R_{eff} as

$$\Delta \ln(COD) = \Delta \ln(LWP) - \Delta ln(R_{eff}). \tag{2}$$

Dividing both sides of the equation by $-\Delta ln(R_{eff})$ we derive a simple metric

$$\frac{\Delta \ln(COD)}{-\Delta \ln(R_{eff})} = 1 - \frac{\Delta \ln(LWP)}{\Delta \ln(R_{eff})} \tag{3}$$

that allows us to compare the total change in COD to the change caused solely by the Twomey effect and ultimately provides a straightforward interpretation of changes in LWP. This ratio has

previously been used by Toll et al. (2019). If the ratio $\frac{\Delta \ln(COD)}{-\Delta \ln(R_{eff})}$ is greater than 1, the LWP has increased since the changes in R_{eff} are always negative. If the ratio is less than 1, the LWP has decreased in polluted areas, resulting in partial compensation of the Twomey effect. If the ratio equals 0, the decrease in LWP entirely cancels the Twomey effect. If the ratio is negative, the LWP decreases so much that the polluted clouds are optically thinner compared to the unpolluted clouds.

2.2 SEVIRI Data

We analyse cloud physical properties derived from SEVIRI instrument data on the Meteosat Second Generation (MSG) satellite. SEVIRI has four visible and near-infrared (VNIR) and eight infrared (IR) channels. In the study area of the European part of Russia, the spatial resolution of the cloud properties product is on average about 10 km by 10 km. The SEVIRI satellite instrument rotates at a rate of 100 rotations per minute, which allows making measurements with 15-minute temporal resolution (Schmid, 2000). Such 15-minute temporal resolution allows to study the temporal evolution of clouds.

We use SEVIRI Cloud Physical Properties (CPP) data (Roebeling et al., 2006). Cloud properties in the CPP product are retrieved in three steps. In the first step, cloud-filled, cloud contaminated, and cloud-free pixels are detected. For the next step, primary cloud properties (Cloud Top Temperature, Cloud Phase, Cloud Optical Thickness and Cloud Droplet Size) are retrieved. For the last step, secondary cloud properties (Cloud Water Path, Cloud Droplet Number Concentration, Cloud Geometrical Thickness, Surface Solar Irradiance, Precipitation occurrence and intensity) are calculated using the values of primary properties achieved in the previous step (Roebeling et al., 2006).

We manually select areas around polluted cloud tracks in SEVIRI data for further analyses. We include only single-layer, liquid-phase and low-level (cloud top lower than 5000 m) clouds and data with the Sun zenith angle less than 80°. We classify the pixels inside the preselected area

around the pollution tracks into polluted and unpolluted pixels depending on cloud droplet size (Fig 3).

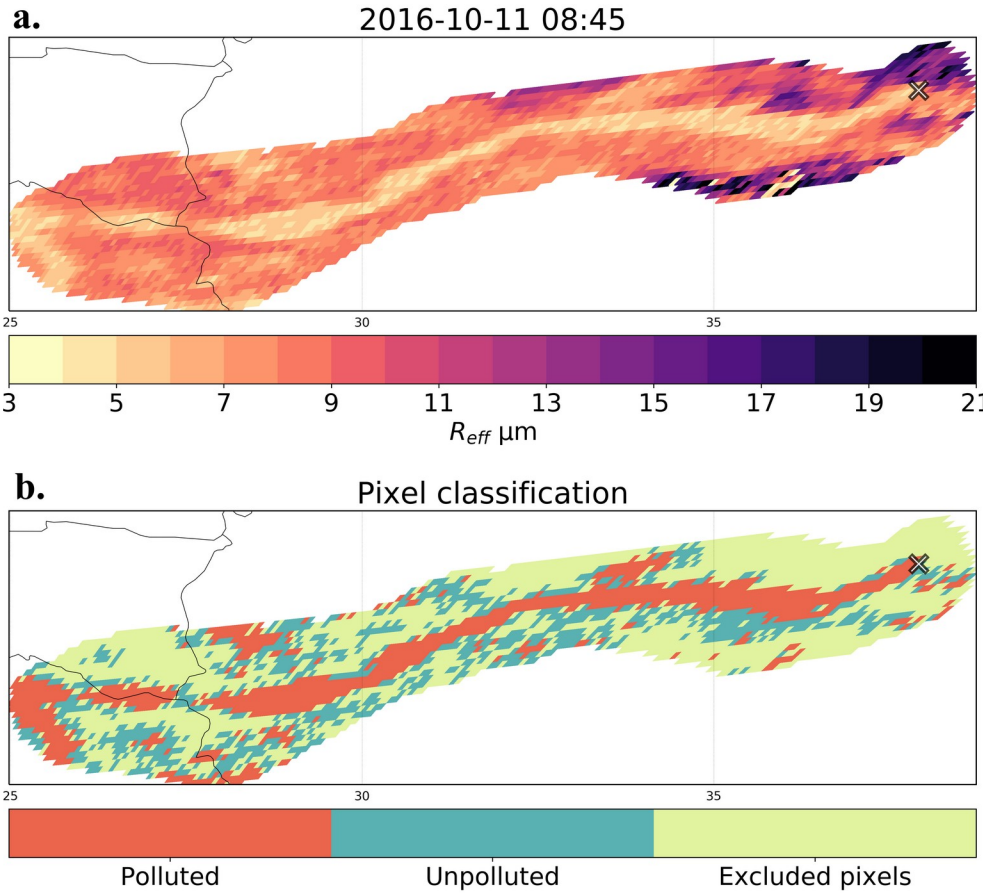

Figure 3. An example of the **a.** manually selected area of one track (top) and **b.** classification of pixels as polluted and unpolluted. Gray cross marks the source of the pollution track.

We classify the pixels in the areas as polluted and unpolluted by selecting the pixels of 25% of the smallest droplet sizes as polluted. Unpolluted pixels stay between the 30th and 55th percentile in droplet size in the masked area, ensuring a roughly similar quantity of pixels in both classes. Due to the CPP algorithm and limitations of the SEVIRI instrument, there were situations where polluted pixels were saturating large areas, causing failures in the first approach. Therefore, additional criteria were introduced to take this issue into account. If the simple counting method resulted in equal or very similar values for the limits of polluted and unpolluted thresholds, the most common value was detected from data (Xth percentile), selected as the polluted pixel threshold. It did not necessarily have to be the 25th percentile, it was usually higher. From that

value, we searched the upper $(X+5)^{th}$ and $(X+30)^{th}$ percentile (still covering the 25-percentile range) to be the unpolluted pixels. Such an approach sometimes introduced discrepancies between the number of classified pixels as the percentile range for polluted values could be greater than 25. If the difference grew too large, the time-series were excluded from the final analysis to minimise the effect of outliers.

Average cloud properties for polluted and unpolluted cloud areas were computed for each timestep. Timeseries of cloud properties thus represent the average values in larger areas (polluted and unpolluted pixels in Fig 3). We included only the cases, where cloud droplet size decreased by at least 20% in the polluted clouds and the total time covered was at least 2 hours. Every timestep was visually inspected for erroneous behaviour in pixel classification and poor data quality. All suspicious timesteps were excluded from the final analysis. In a few cases, there were unexplainable fast and large increases (spikes) in LWP values in SEVIRI data which we considered as errors in data and excluded from the analysis. Also, if the areas consisted of very few pixels (less than 100 pixels), they were excluded. With these additional criteria, we excluded 50.7% of initial data points from the analysis. We checked that the results were not sensitive to the data screening.

The difference in the spatial resolution between SEVIRI and MODIS instruments is significant (~10 km vs 1 km, respectively), but only SEVIRI data enables to study the temporal evolution of clouds. Due to lower spatial resolution, the contrast between relatively narrow polluted and unpolluted areas is lower.

2.3 Moderate Resolution Imaging Spectroradiometer (MODIS) data

Diurnal evolution of cloud response to aerosols was also studied, based on MODIS data for polluted cloud tracks. The MODIS data used here have been previously sampled by Toll et al. (2019). MODIS level 2 cloud products (MOD06_L2 for Terra and MYD06_L2 for Aqua) were used. The dataset included 8379 different pollution track segments over Russia, Australia, and Canada, observed in various seasons. Details of MODIS data screening and classification of MODIS pixels as polluted and unpolluted is given in Toll et al. (2019). Single-layer liquid-water

low-level clouds were studied similarly to SEVIRI data which was newly sampled for this study. For each MODIS image, where the polluted cloud track was visually detected, the centreline of the polluted cloud track was manually sampled, and pixels around this line were classified as polluted or unpolluted, based on near-infrared reflectance using a semi-automated algorithm (Toll et al., 2019). The polluted cloud tracks were sampled for various local times by Toll et al. (2019) so that using all MODIS cases from Terra and Aqua for various locations, continuous temporal coverage between sunrise and sunset is derived. MODIS data consists of snapshots of many pollution tracks from various geographical areas. Therefore, MODIS data does not enable us to study the temporal evolution of the individual pollution tracks. Using SEVIRI data, we study the temporal evolution of individual pollution tracks in time.

3 Results

We have found that SEVIRI data is useful for studying polluted cloud tracks. Although the spatial resolution is roughly about 10 times worse for SEVIRI data (about 10 km at given latitude) compared to MODIS data (1 km), we were still able to effectively detect the pollution tracks. In SEVIRI data, similarly to MODIS data, there is a clear contrast between polluted and unpolluted clouds (Fig 2 and Fig 3). On average, the cloud droplet size of the polluted clouds was 27% smaller compared to the nearby less polluted clouds (Table 3).

Table 3. Average values of cloud optical properties over all the data (2 leftmost columns) and averages for the orange and green groups from Fig 6. The orange group includes cases with strong liquid water path (LWP) increase and the green group includes all the other cases. Averages for cloud droplet effective radius (R_{eff}), LWP and cloud optical depth (COD) together with the standard deviation in the parentheses.

	Polluted	Unpolluted	Polluted Strong increase cases	Unpolluted Strong increase cases		Polluted other cases	Unpolluted other cases

R_{eff} (μm)	5.8 (1.4)	7.9 (2.0)	5.3 (0.4)	7.2 (0.6)		6.0 (1.6)	8.1 (2.2)
LWP $\left(\frac{g}{m^2}\right)$	58.6 (32.8)	68.1 (34.8)	65.1 (36.9)	49.3 (20.5)		56.3 (30.9)	74.8 (36.3)
COD	15.1 (7.2)	12.6 (4.6)	18.9 (11.0)	10.3 (4.2)		13.7 (4.5)	13.4 (4.5)

Based on both MODIS and SEVIRI data, there is a partial offset of the Twomey effect due to the decrease in cloud water. The mean value of $\frac{\Delta \ln(COD)}{-\Delta \ln(R_{eff})}$ for MODIS data is 0.74, meaning that on average decrease in LWP offsets 26% of the Twomey effect. The mean value of $\frac{\Delta \ln(COD)}{-\Delta \ln(R_{eff})}$ for SEVIRI data is 0.54, meaning that on average decrease in LWP offsets 46% of the Twomey effect. Data-points are not distributed evenly throughout the day. In the case of both MODIS and SEVIRI data, we have the largest number of cases around noontime (Fig 4). Due to poor lighting conditions in the very early morning and very late evening, there is only a limited number of data points during these times (Fig 4). Most of the day is still sufficiently covered for both instruments.

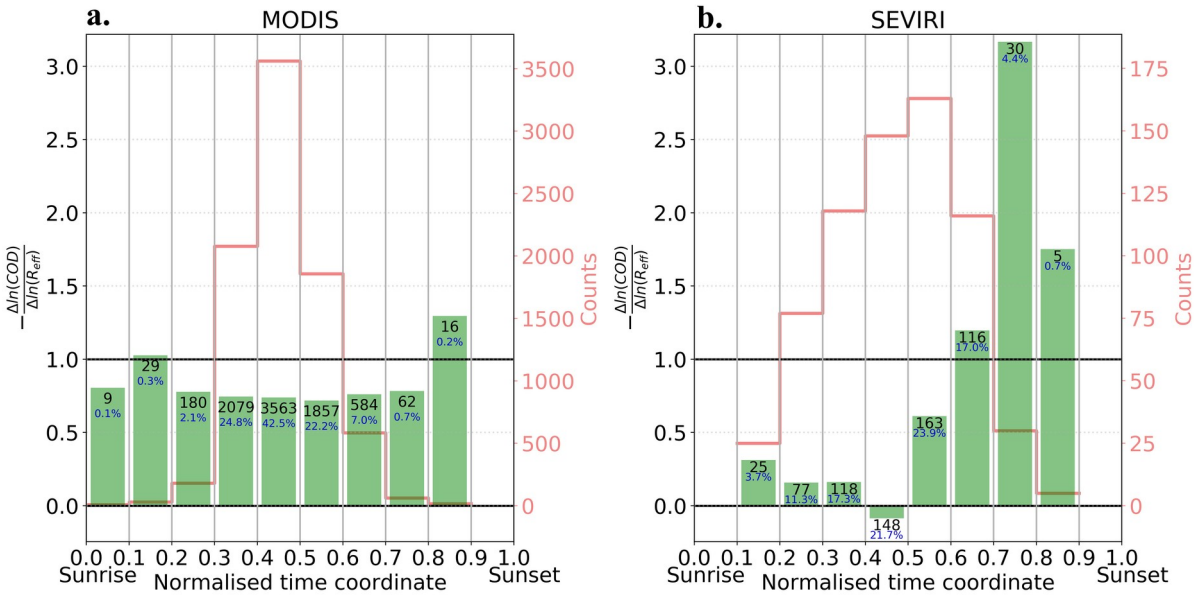

Figure 4. Average changes in $\frac{-\Delta ln(COD)}{\Delta ln(R_{eff})}$ (green) distributed over normalised time coordinate from sunrise (0.0) to sunset (1.0). The time coordinate value of 0.5 represents the local noon. Total counts of data points are given in black with relative occurrence in blue (at the top of each column) and graphically in red on the second y-axis. **a.** MODIS cases and **b.** SEVIRI cases included in the study. Both based on MODIS and SEVIRI data, decrease in cloud water offsets part of the Twomey effect. There is no clear diurnal evolution in liquid water path (LWP) response based on MODIS data. Based on SEVIRI data, cloud water is more likely to increase in the afternoon.

MODIS and SEVIRI data reveal day-night contrast in the cloud water response to cloud droplet number perturbations. MODIS data shows a uniformly weak decrease in cloud water during sunlight hours, while SEVIRI data shows a substantial decrease in the morning and increase in the afternoon (Fig 4). Both MODIS and SEVIRI data show decreased cloud water since the sunrise, suggesting that a decrease in cloud water occurs during the night, potentially through aerosol-enhanced entrainment. In the afternoon, increased cloud water in the polluted clouds is found in SEVIRI data (Fig 4 and Fig 5). This strong increase is caused by cases where cloud water in polluted clouds increases in the afternoon much more than in the unpolluted clouds, most probably due to suppressed precipitation in the polluted clouds (Fig 5 and Fig 6).

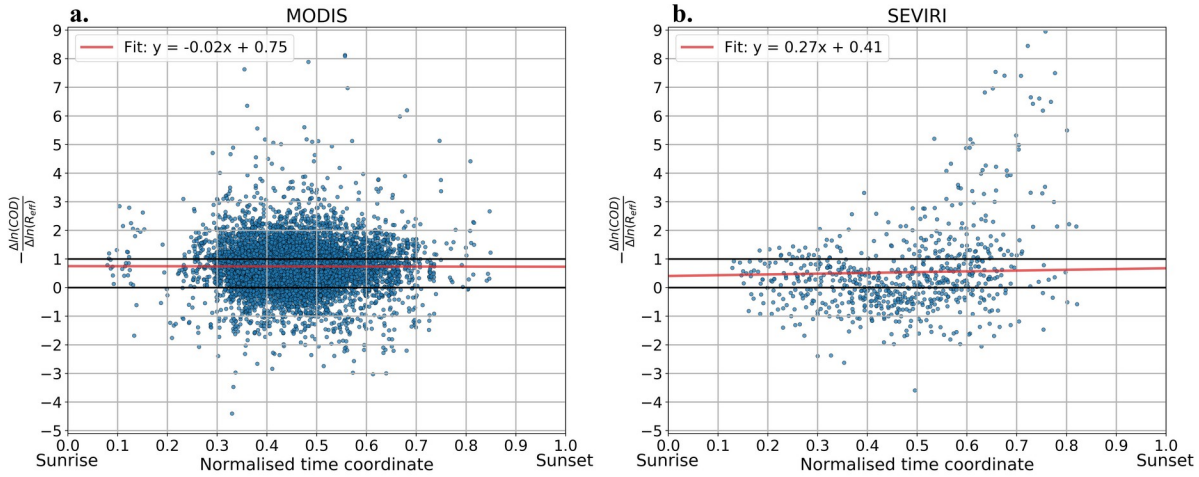

Figure 5. The ratio $\frac{-\Delta ln(COD)}{\Delta ln(R_{eff})}$ scattered over normalised time coordinate from sunrise (0.0) to sunset (1.0). The time coordinate value of 0.5 represents the local noon. **a.** MODIS cases (8379

in total) and **b.** SEVIRI cases (682 in total) included in the study. Red lines are least-square fits to the data points. Decrease in cloud water offsets part of the Twomey effect in both datasets. In SEVIRI data, a considerable number of data points with strongly increased liquid water path (LWP) in the afternoon are seen, while no cases with such strong increases in LWP are seen in the morning.

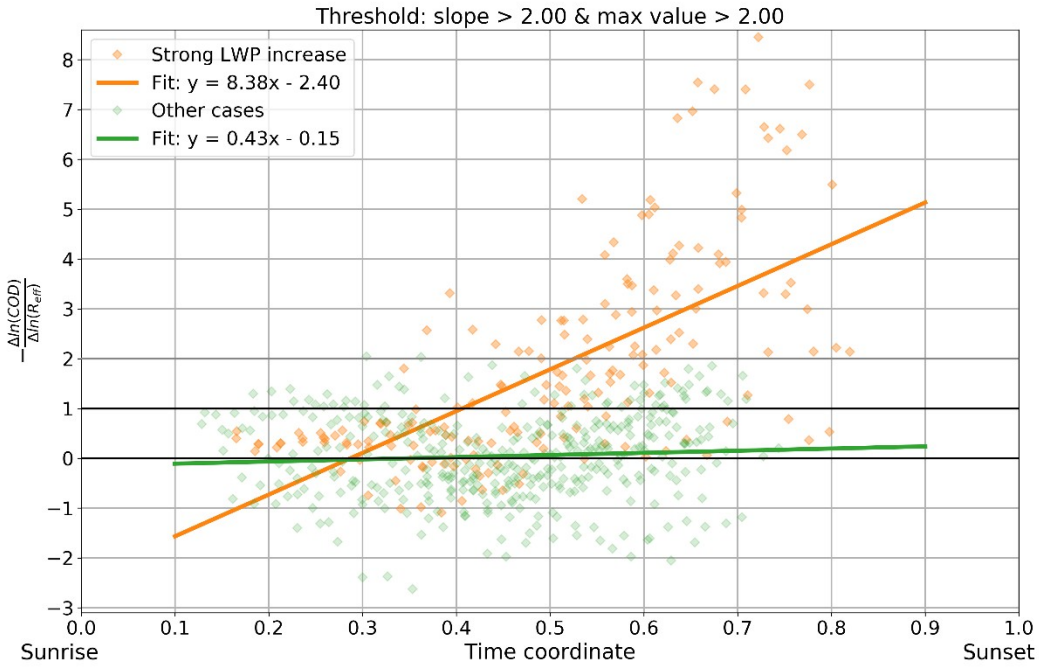

Figure 6. SEVIRI time-series of individual tracks classified into two groups. The orange group includes cases with strong liquid water path (LWP) increase and the green group includes all the other cases. The most plausible physical interpretation is that the orange group includes cases with suppressed precipitation in the polluted clouds. The following criteria were used to select cases in the orange group: slopes of linear fits are greater than 2.0 and that the maximum value of the ratio $\frac{-\Delta ln(COD)}{\Delta ln(R_{eff})}$ is greater than 2.0. The orange group shows that the increase in LWP happens in the afternoon. The green group indicates that the decrease in LWP has already occurred during the night and no further decrease occurs during the day in the polluted cloud tracks.

We found two groups of pollution tracks with very different temporal evolutions of the cloud water response in SEVIRI data. Most likely, these groups include cases with suppressed precipitation in polluted clouds and all other cases, respectively. The cases in the orange group in Fig 6 show strong increases in LWP in the afternoon and these are likely the cases where precipitation is suppressed in the polluted clouds compared to the unpolluted clouds. The orange group includes thinner unpolluted clouds. The average LWP for unpolluted clouds within the orange group is $49.3\,\frac{g}{m^2}$ while for the other cases, it is $74.8\,\frac{g}{m^2}$. In the orange group, only the polluted clouds can become much thicker during the day.

In cases, where precipitation in polluted clouds is not suppressed compared to the unpolluted clouds (green group in Fig 6), no apparent change in cloud water response is observed during the sunlight hours. Only three individual tracks were detected, where the cloud water response became more negative during the sunlight hours, which strongly supports the hypothesis that cloud water decreases during the night due to aerosol-enhanced entrainment. In most cases, the LWP of polluted clouds is much lower already at sunrise. For the orange group, the increase in LWP enhances the Twomey effect by 80% on average. For the green group, the decrease in LWP offsets 95% of the Twomey effect.

4 Discussion and Conclusions

We demonstrated that SEVIRI data could be used to study the temporal evolution of polluted cloud tracks. SEVIRI data shows that on average the decrease in cloud water offsets 46% of the Twomey effect in the European part of Russia. The partial offset of the Twomey effect is in good agreement with the analysis of MODIS data by Toll et al (2019) and Trofimov et al (2020). As the number of data points for SEVIRI data is much more limited and only a single geographical region is studied, the average cloud water response is likely to be much less representative of the global average cloud water response than the MODIS dataset included in this study. But the temporal evolution from SEVIRI data helps to increase the process-level understanding of aerosol-cloud interactions.

SEVIRI data reveals day-night contrast in the cloud water response to aerosols. In some cases, cloud water strongly increases in the polluted clouds compared to the unpolluted clouds in the afternoon, most likely due to the suppression of precipitation. In most cases, cloud water is decreased in the polluted clouds since the early morning and no further decrease compared to the unpolluted clouds is observed during the day (Fig 6). This suggests that cloud water decreases more in the polluted clouds during the night-time, probably due to aerosol-enhanced entrainment. However, as SEVIRI provides only day-time data, we can only speculate how the cloud water responds during night-time. Our results show that the temporal evolution of cloud responses to aerosols is very important to consider in aerosol radiative forcing calculations.

Our results disagree with Diamond et al. (2020) who found a more substantial decrease in cloud water in the afternoon compared to the morning in the South-East Atlantic shipping corridor. A possible explanation with the disagreement with Diamond et al. (2020) is that land-based tracks analysed in this study could behave differently compared to the ocean-based tracks analysed by Diamond et al. (2020). In the future, we plan to use SEVIRI data to analyse the temporal evolution of ship tracks to compare track responses over land and ocean. Interestingly, an increase in LWP during a later stage of track evolution in the afternoon agrees with the ship track analysis by Gryspeerdt et al. (2020) and Christensen et al. (2009). Segrin et al. (2007) found a rather similar decrease in LWP in ship tracks in the morning and afternoon.

Our finding that LWP decreases more in the polluted clouds than in the unpolluted clouds only during the night-time disagrees with process-level modelling by Sandu et al (2008). Sandu et al. (2008) suggested that the decrease in cloud water is amplified during the day (Sandu et al. 2008). Glassmeier et al. (2021) discuss that ship tracks are not suitable to inform calculations of radiative forcing due to the short lifetime of the tracks. We plan to study the lifetime of pollution tracks in more detail in future work, but the lifetime of the polluted cloud tracks studied here spans from less than a single day to multiple days. We find no further decrease in LWP of polluted clouds compared to the nearby unpolluted clouds during the daytime also for shorter-lived tracks. This suggests that polluted clouds could reach an equilibrium state quicker than 20 hours suggested by Glassmeier et al. (2021). Moreover, Glassmeier et al. (2021) might

351 overestimate the decrease in cloud water of non-precipitating clouds as they use only nocturnal
352 radiation in their simulations. Our results highlight the need to account for the day-night contrast
353 in the cloud responses as the night-time responses are not representative of the average response.
354

355 **Acknowledgements and data availability**

356

357 This study was funded by the Estonian Research Council personal research funding grant
358 PSG202. We used Cloud Physical Properties derived from SEVIRI data as provided by KNMI at
359 https://dataplatform.knmi.nl. The MODIS cloud products MYD06_L2 from Aqua and
360 MOD06_L2 from Terra used in this study are available from the Atmosphere Archive and
361 Distribution System (LAADS) Distributed Active Archive Center (DAAC),
362 https://ladsweb.nascom.nasa.gov/.

363 **Author contributions**

364 VT designed the study. JR identified the polluted cloud areas in SEVIRI satellite images and
365 analysed the observations. HT analysed MODIS satellite data. JR and VT wrote the manuscript
366 with contributions from HT and PP.

367

368 **References**

369

370 Ackerman, A. S., Kirkpatrick, M. P., Stevens, D. E., & Toon, O. B. (2004). The impact of
371 humidity above stratiform clouds on indirect aerosol climate forcing. *Nature 432*(7020),
372 1014–1017. https://doi.org/10.1038/nature03174

373 Albrecht, B. A. (1989). Aerosols, Cloud Microphysics, and Fractional Cloudiness. *Science*
374 *245*(4923), 1227–1230. doi: 10.1126/science.245.4923.1227

375 Bellouin, N., Quaas, J., Gryspeerdt, E., Kinne, S., Stier, P., Watson−Parris, D., et al. (2020).
376 Bounding Global Aerosol Radiative Forcing of Climate Change. *Reviews of Geophysics*
377 *58*(1), e2019RG000660. https://doi.org/10.1029/2019RG000660

378 Bretherton, C. S., Blossey, P. N., & Uchida, J. (2007). Cloud droplet sedimentation, entrainment
379 efficiency, and subtropical stratocumulus albedo. *Geophysical Research Letters 34*(1),
380 L03813. doi: 10.1029/2006GL027648

Diamond, M. S., Director, H. M., Eastman, R., Possner, A., & Wood, R. (2020). Substantial Cloud Brightening from Shipping in Subtropical Low Clouds. *AGU Advances 1*(1), e2019AV000111. https://doi.org/10.1029/2019AV000111

Ghan, S., Wang, M., Zhang, S., Ferrachat, S., Gettelman, A., Griesfeller, J., et al. (2016). Challenges in constraining anthropogenic aerosol effects on cloud radiative forcing using present-day spatiotemporal variability. PNAS 113(21), 5804–5811. https://doi.org/10.1073/pnas.1514036113

Glassmeier, F., Hoffmann, F., Johnson, J. S., Yamaguchi, T., Carslaw, K. S., & Feingold, G. (2021). Aerosol-cloud-climate cooling overestimated by ship-track data. *Science 371*(6528), 485–489. doi: 10.1126/science.abd3980

Gryspeerdt, E., Goren, T., & Smith, T. W. P., (2020), Observing the timescales of aerosol-cloud interactions in snapshot satellite images (preprint). Clouds and Precipitation/Remote Sensing/Troposphere/Physics (physical properties and processes). https://doi.org/10.5194/acp-2020-1030

IPCC, 2013. Climate Change 2013: The Physical Science Basis. Contribution of Working Group I to the Fifth Assessment Report of the Intergovernmental Panel on Climate Change. Stocker, T.F., D. Qin, G.-K. Plattner, M. Tignor, S.K. Allen, J. Boschung, A. Nauels, Y. Xia, V. Bex and P.M. Midgley (eds.), Cambridge University Press, Cambridge, United Kingdom and New York, NY, USA.

Roebeling, R. A., Feijt, A. J., & Stammes, P. (2006). Cloud property retrievals for climate monitoring: Implications of differences between Spinning Enhanced Visible and Infrared Imager (SEVIRI) on METEOSAT-8 and Advanced Very High Resolution Radiometer (AVHRR) on NOAA-17. *J. Geophys. Res. 111*, D20210. https://doi.org/10.1029/2005JD006990

Schmid, J. (2000). *The SEVIRI Instrument*. Paper presented at The 2000 EUMETSAT Meteorological Satellite Data Users' Conference, EUMETSAT, Bologna, Italy.

Stevens, B., Sherwood, S. C., Bony, S., & Webb, M. J. (2016). Prospects for narrowing bounds on Earth's equilibrium climate sensitivity. *Earth's Future 4*(11), 512–522. https://doi.org/10.1002/2016EF000376

Toll, V., Christensen, M., Gassó, S., & Bellouin, N. (2017). Volcano and Ship Tracks Indicate Excessive Aerosol-Induced Cloud Water Increases in a Climate Model. *Geophysical Research Letters 44*(24), 12,492-12,500. https://doi.org/10.1002/2017GL075280

Toll, V., Christensen, M., Quaas, J., & Bellouin, N. (2019). Weak average liquid-cloud-water response to anthropogenic aerosols. *Nature 572*, 51–55. https://doi.org/10.1038/s41586-019-1423-9

Trofimov, H., Bellouin, N., & Toll, V. (2020). Large-Scale Industrial Cloud Perturbations Confirm Bidirectional Cloud Water Responses to Anthropogenic Aerosols. *Journal of Geophysical Research: Atmospheres 125*(14), e2020JD032575. https://doi.org/10.1029/2020JD032575

Twomey, S. (1974). Pollution and the planetary albedo. *Atmospheric Environment 8*(12), 1251–1256. https://doi.org/10.1016/0004-6981(74)90004-3

Wood, R. (2007). Cancellation of Aerosol Indirect Effects in Marine Stratocumulus through Cloud Thinning. *Journal of the Atmospheric Sciences 64*(7), 2657–2669. https://doi.org/10.1175/JAS3942.1